수의학석사학위논문

저용량 레이저 치료가 무세포성 진피 기질에 배양된 개 지방유래 중간엽줄기세포의 골재생에 미치는 영향

Low-level Laser Therapy Promotes the Osteogenic Potential of Adipose-derived Mesenchymal Stem Cells Seeded on an Acellular Dermal Matrix in Athymic Mice

2013 년 8 월

서울대학교 대학원

수의학과 수의외과학 전공

최 규 석

저용량 레이저 치료가 무세포성 진피 기질에 배양된 개 지방유래 중간엽줄기세포의 골재생에 미치는 영향

Low-level Laser Therapy Promotes the Osteogenic Potential of Adipose-derived Mesenchymal Stem Cells Seeded on an Acellular Dermal Matrix in Athymic Mice

지도교수 김 완 희

이 논문을 수의학석사학위논문으로 제출함
2013 년 4 월

서울대학교 대학원
수의학과 수의외과학 전공
최 규 석

최규석의 석사학위논문을 인준함.
2013 년 6 월

위 원 장 _____ (인)
부위원장 _____ (인)
위 원 _____ (인)

Low-level Laser Therapy Promotes the Osteogenic Potential of Adipose-derived Mesenchymal Stem Cells Seeded on an Acellular Dermal Matrix in Athymic Mice

Director: Associate Professor Wan Hee Kim

Kyuseok Choi

Major in Veterinary Surgery

Department of Veterinary Medicine

Graduate School

Seoul National University

Abstract

An adipose-derived mesenchymal stem cell (ASC)-seeded acellular dermal matrix (ADM) has been used for bone regeneration. Additionally, numerous studies have

demonstrated that low-level laser therapy (LLLT) affects bone repair in experimental animals. This study investigates the feasibility of using an ASC-seeded ADM along with LLLT to repair bone defect in athymic nude mice.

Critical-sized calvarial defects were treated either with an ADM (ADM group), an ADM along with LLLT (ADM/LLLT group), an ASC-seeded ADM (ADM/ASCs group) or an ASC-seeded ADM along with LLLT (ADM/ASCs/LLLT group). The animals were euthanized at 3, 7, 14, 21, 28 and 56 days. Micro-computed tomographic (CT) imaging, histological evaluation, immunohistochemistry and western blot were performed.

In micro-CT images, the ADM/ASCs and the ADM/ASCs/LLLT groups showed remarkable bone formation after 14 days. Furthermore, bone regeneration in the ADM/ASCs/LLLT group was obvious at 28 days, but in the ADM/ASCs group at 56 days. Bone mineral density (BMD) and bone tissue volume (BTV) in the ADM/ASCs/LLLT group significantly increased after 7 days, but in the ADM/ASCs group after 14 days. Histological analysis revealed that the defects were repaired in the ADM/ASCs and the ADM/ASCs/LLLT group, while the defects in the ADM and the ADM/LLLT groups exhibited few bone islands with fibrous connection at 28 and 56 days. The successful seeding of ASCs onto ADM was confirmed, and LLLT enhanced the proliferation and the survival of ASCs at 14 days.

An ASC-seeded graft promoted bone regeneration, and the application of LLLT on an ASC-seeded ADM results in rapid bone formation. The implantation of an ASC-seeded ADM combined with LLLT may be used effectively for bone regeneration.

Keywords: Low-level laser therapy (LLLT), Adipose-derived mesenchymal stem cells (ASCs), Acellular dermal matrix (ADM), Bone regeneration, Athymic mice, Scaffold

Student Number: 2010 - 21634

CONTENTS

I. Introduction

Skeletal tissue defects can be successfully repaired by using either autogenous grafts or alloplastic materials. Autogenous bone grafts still provide the best clinical outcome, but require a substantive operation with potential morbidity (Cui et al. 2007, Khan et al. 2005). Allogenic transplants also have problems with poor quality, rejection, and disease transmission from the donor to the recipient (Ye et al. 2011, Zuk et al. 2002). Thus, there remains a pressing need for a suitable alternative to the currently available techniques for bone tissue repair. Our laboratory and others have focused on utilizing the osteogenic potential of adipose-derived mesenchymal stem cells (ASCs) for the eventual repair of skeletal defects (Kim et al. 2012b). ASCs isolated noninvasively from the lipoaspirate offer several advantages over other multipotent cells and are considered an attractive source of cells for tissue engineering applications (Cui et al. 2007, Gupta et al. 2008, Zuk et al. 2002). ASC-seeded grafts have been used for the bone regeneration to repair skeletal defects, and the *in vivo* osteogenic capability of ASCs placed extraskeletally has been described (Meinel et al. 2005).

Biological materials composed of an acellular dermal matrix (ADM) that was derived

from a human cadaveric dermis offer many advantages over synthetic materials, including very low antigenicity, excellent stability and favorable handling properties, and can thus usually be used to treat bone defects. A biological scaffold offers an advantage for introducing stem cells to the recipient, as it supplies a framework to support their regenerative capacity. Furthermore, an ADM, as a three-dimensional structure, has surface polarity that enables the growth of stem cells and resists cellular migration (Kim et al. 2012b, Schönmeyr et al. 2009). The use of an ADM may be a more suitable choice compared with synthetic biodegradable scaffolds.

Our laboratory has previously demonstrated an athymic murine calvarial defect model for the use of ASCs grown on an ADM to heal the critical-sized defects (Kim et al. 2012b). In 3D images, new bone formation in the ADM/ASCs group was apparent at 28 days, but in the ADM group at 56 days. Furthermore, histological examination showed that the defect was repaired by bone in the ADM/ASCs group, whereas only mineral bone island with fibrous connection was observed in the control group. However, our previous study could not evaluate an initial phase of bone regeneration before 28 days and had a limited ability to quantify the osteogenic markers. In the present study, we examined an early phase of bone regeneration by 3D imaging and histological analysis, and quantified the osteogenic markers

at 3, 7, 14, 21, 28 and 56 days.

Additionally, we examined whether an augmentation of osteogenic healing of ASCs was observed by supplementation with low-level laser therapy (LLLT). LLLT is a simple atraumatic technique that has been used for various purposes. Numerous studies have demonstrated that LLLT affects bone repair in experimental animals following trauma and stimulates cellular response and proliferation (Abramovitch-Gottlib et al. 2005, Hou et al. 2008, Mvula et al. 2008, Yaakobi et al. 1996). However, some experimental and clinical studies have evaluated the effects of LLLT on the process of tissue regeneration with contradictory results; furthermore, there are few investigations about the effects of LLLT on ASCs in animal studies (Amaral et al. 2001).

Herein, we evaluated the possible role of ASC-seeded ADM at initial phase of bone regeneration processes and assessed the effect of LLLT on an implanted ASC-seeded ADM.

II. Materials and Methods

1. Culture and labeling of canine ASCs

Canine ASCs used in this study were previously isolated and characterized (Ryu et al. 2009). These canine ASCs were used for research about the regeneration of skin, spinal cord and bone in our previous study (Kang et al. 2012, Kim et al. 2012a, Kim et al. 2012b, Park et al. 2012, Ryu et al. 2009). The ASCs were cultured at passages 2 to 3, and chloromethylbenzamido-1,1'-dioctadecyl-3,3,3'3'- tetramethylindocarbocyanine perchlorate (CellTracker™ CM-DiI, C7000, Molecular Probes™, Eugene, OR, USA) was used for the labeling of the ASCs according to the manufacturer's instructions. Briefly, CM-DiI was dissolved in 1 mg/mL dimethyl sulphoxide (DMSO) and added to the adherent ASCs such that the final concentration was 20 μg/mL.

2. Preparation of CM-DiI-labeled ASC-seeded grafts *in vitro*

The ADM scaffold produced from human dermal tissue was obtained from a commercial supplier (SureDerm™, ADM 102008, Hans Biomed, Seoul, Korea). The ADM was cut with a dermal punch biopsy instrument (Biopsy Punch REF 33-34, Miltex, PA, USA) to the shape of a disk with a diameter of 4 mm. Each piece was incubated with fresh 50 μL

medium alone or with a suspension of 1×10^5 of CM-DiI-labeled ASCs suspended in 50 μL medium at 37℃ in a humidified chamber containing 5% CO_2 for 24 hours. The ADMs were removed from culture conditions and were placed with the opposite side facing upward. The ADM grafts were covered with the same volume of the fresh medium alone or the cell suspension and were incubated for an additional 24 hours. The cell attachment to the ADM was checked by identifying nuclei to determine the ASCs seeding density. The ADM grafts were then removed from culture conditions for sterile transport to the surgical suite for operative engraftment.

3. Scanning electron microscopy

The ADM was examined using scanning electron microscopy (SEM). The ADM and the ASC-seeded ADM were fixed in modified Karnovsky's fixative [2% paraformaldehyde and 2% glutaraldehyde in 0.05 M sodium cacodylate buffer (pH 7.2)]. Post-fixation in 1% osmium tetroxide in 0.05 M sodium cacodylate buffer was followed by dehydrating in a graded ethanol series and drying using hexamethyldisilazane. The specimens were mounted on metal stubs and coated with platinum in a dc sputter coater. The samples were examined using an AURIGA field-emission scanning electron microscope (Carl Zeiss, Oberkochen, Germany).

4. Calvarial defects procedure for the experimental animal model

Seventy-two 7-week-old male athymic nude mice (BALB/cSlc-*nu/nu*) weighing 15-17 g each were obtained from Japan SLC Inc. (Shizuoka, Japan). All animal procedures including the care, maintenance and treatment of the mice were approved by the Institutional Animal Care and Use Committee (IACUC) of Seoul National University (SNU-120106-5). Experimental animals were anesthetized with an intraperitoneal injection of 30 mg/kg of tiletamine HCl/zolazepam HCl (Zoletil®, Virbac, Carros, France) and 10 mg/kg of xylazine (Rompun®, Bayer Korea, Suwon, Korea). Supplemental injection of 22 mg/kg of cefazolin (cefazolin sodium, Chong Kun Dang Pharmaceutical, Seoul, Korea) and 2 mg/kg of tramadol (Toranzin®, Shinpoong, Seoul, Korea) were both given intraperitoneally to prevent infection and to relieve pain. The dorsal part of the calvarium was cleaned aseptically for surgery. Two full-thickness, 4-mm-diameter critical-sized calvarial defects were trephined in the dorsal part of the bilateral parietal bone lateral to the sagittal midline suture. A 4-mm external diameter trephine bur (Trepan bur 227A 204 040, Komet® Gebr. Brasseler GmbH & Co. KG, Lemgo, Germany) attached to a high-speed hand piece was used to create the defects, and extreme care was taken to prevent invasion into the dura mater and the brain. After the 4-mm bone disk was carefully peeled away and discarded. The ADM was then carefully placed into the defect using sterile forceps. The defects were classified into four

groups randomly: ADM, ADM/LLLT, ADM/ASCs and ADM/ASCs/LLLT groups. The ADM was placed into both the ADM and the ADM/LLLT groups, and ASC-seeded ADM was placed into both the ADM/ASCs and the ADM/ASCs/LLLT groups. The scalp was then immediately sutured in an interrupted fashion. Animals were monitored according to established post-operative animal care protocols. Neither wound infections nor post-operative mortality was observed.

5. Low-level laser therapy

A helium-neon laser (He-Ne cold laser stimulator model PDT-A2, Lead Medical Science, Japan) with a continuous wavelength of 632.8 nm (output power of 17.0 mW) was delivered to a calvarial defect of 4-mm diameter through a hole in a wrinkled aluminum foil wrapping the dorsal part of the calvarium. The aluminum foil served for extensively reflecting the laser beam and uniformly irradiating the whole calvarial defect (Abramovitch-Gottlib et al. 2005). *In vitro* pilot experiment was performed to find the appropriate dose of LLLT to ASCs, and viable cell number of ASCs significantly increased in the group irradiated with the 1 J/cm^2 compared with 0 and 3 J/cm^2 ($p < 0.05$) (data is not shown). In conclusion, the defect was irradiated by the laser beam from a distance of 10 mm for 8 seconds daily from days 0 to 56. The employed power density of each defect was 0.136

J/defect and approximately 1.083 J/cm^2. The non-irradiation group of defects was maintained under similar conditions but without irradiation.

6. Three-dimensional (3D) micro computed tomography

At 3, 7, 14, 21, 28 and 56 days, mice were euthanized by CO_2 asphyxiation, and the calvarial defects were harvested. The samples were imaged by micro-computed tomography (micro-CT), using a high-resolution SkyScan 1172 micro-CT scanner (SkyScan, Kontich, Belgium). Every sample was scanned with a CT-phantom, and the isosurface was set in Hounsfield units according to the phantom, which included hydroxyapetite, water and air. The 3D reconstructions and quantified data were analyzed with a commercial software package [NRecon, DATA-VIEWER, CTAn (v.1.11) and CTVol (v.2.1)].

7. Histological and immunofluorescence assessment

One half of each calvarial defect harvested was fixed in 10% formalin, decalcified in 8% nitric acid, and embedded in paraffin. The other half was immediately frozen with liquid nitrogen for western blot analysis. The portion closest to the central part of each defect was subjected to histological analysis. Serial sections (4-μm-thickness) parallel to the midsagittal suture were stained with hematoxylin and eosin (H&E). To detect the osteoclasts, tartrate-

resistant acid phophatase (TRACP) staining was carried out using the TRACP & ALP double-stain kit (TAKARA Bio Inc., Shiga, Japan) according to the manufacturer's instructions. The following primary antibodies were used in immunohistochemistry: rabbit anti-bone alkaline phosphatase (bALP) antibody (1:250, ab108337, Abcam, Cambridge, UK), rabbit anti-osteopontin (OPN) antibody (1:100, ab8448, Abcam) and rabbit anti-osteocalcin (OCA) antibody (1:200, ab93876, Abcam). The slides that reacted with each of the primary antibodies were exposed to horseradish peroxidase (HRP)-conjugated goat anti-rabbit IgG (1:200, G21234, Molecular Probes™, Eugene, OR, USA) and were visualized by a reaction with 3,3'-diaminobenzidine (DAB) tetrahydrochloride (D5637, Sigma, St. Louis, MO, USA). The procedure was completed by hematoxylin counterstaining. To confirm the proliferation and the survival of the ASCs on the graft, some sections were processed for immunofluorescence staining. These sections were incubated with rabbit anti-Ki67 antibody (1:125, ab15580, Abcam) and were then incubated with Alexa Fluor® 488-conjugated goat anti-rabbit IgG (1:100, A11008, Molecular Probes™). DAPI (4,6-diamidino-2-phenylindole) was used for nuclear staining. In addition, the other sections were stained using the TUNEL Apoptosis detection kit (L00300, GenScript, Piscataway, NJ, USA) according to the manufacturer's instruction. The immunoreactions were observed under a LSM700 confocal laser scanning microscope (Carl Zeiss, Oberkochen, Germany). The percentages of Ki67-,

TUNEL-positive ASCs were determined by counting Ki67-, TUNEL-positive ASCs and total ASCs in five random fields per section.

8. Western blot analysis

The frozen half of each calvarial defect was homogenized in a protein extraction solution and a protease inhibitor cocktail. After the lysates were centrifuged, their protein concentrations were determined using the Bradford method. Aliquots containing 30 μg of total protein were separated by 10% or 15% SDS-polyacrylamide gel electrophoresis and transferred onto transfer membranes. The membranes were incubated with the primary antibodies: bALP (1:1,000, ab108337, Abcam), OPN (1:1,000, ab8448, Abcam), OCA (1:500, ab10911, Millipore, Temecula, CA, USA), TRACP (1:2,000, ab96372, Abcam) and β–actin (1:1,000, sc47778, Santa Cruz Biotechnology, USA). As a secondary antibody, HRP-conjugated goat anti-rabbit IgG (1:5,000, G21234, Molecular Probes™) or HRP-conjugated goat anti-mouse IgG (1:5,000, G21040, Molecular Probes™) was used, the immunoreactive protein was subsequently visualized using an enhanced luminol-based chemiluminescent kit (ECL kit, Invitrogen, USA). The blot was densitometrically scanned for quantification of the relative optical intensity of each band using ImageJ software (NIH Image).

9. Statistical Analysis

The mean and standard deviations were calculated from numerical data. In the figures, bar graphs and error bars represent the mean and standard deviation, respectively. Statistical analysis was performed by one-way analysis of variance (ANOVA), and Tukey's HSD test was used for comparisons between the groups. Independent t-test was used for the proliferation and the survival of the ASCs in the grafts, if necessary, using the software SPSS, version 19.0 (SPSS Inc. DE, USA). A p value less than 0.05 was considered significant.

III. Results

1. SEM analysis

The adhesion of the CM-DiI-labeled ASCs to the ADM was confirmed using SEM analysis. Examination of the unseeded control ADM showed the relatively smooth undulating topography of the ADM (Fig. 1a). In contrast, the CM-DiI-labeled ASC-seeded ADM revealed that adherent ASCs were spread uniformly. Furthermore, fibrillar projections of ASCs were anchored to the surface of the ADM (Fig. 1b).

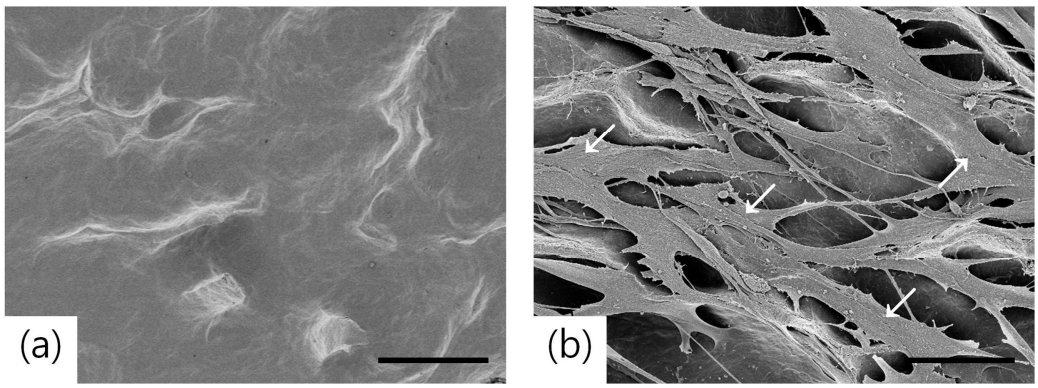

Fig. 1. SEM analysis. Typical SEM appearance of the unseeded control ADM (a) and the ASC-seeded ADM for 24 h (b). Adherent ASCs are spread uniformly to the surface of the ADM, and some of them are indicated by arrows in the ASC-seeded ADM (b) (Scale bar = 100 μm).

2. Micro-CT evaluation

The ADM and the ADM/LLLT groups exhibited little osseous healing in the marginal region and few bone islands in a small percentage of defects at 56 days. In comparison, the defects in the ADM/ASCs and the ADM/ASCs/LLLT groups showed that new bone formation was advanced after 14 days. The ADM/ASCs group exhibited an advancement of bone regeneration and robust healing at 56 days. The ADM/ASCs/LLLT group defects were covered with thicker layers of regenerated bone, and almost complete bone closure was apparent at 28 days (Fig. 2).

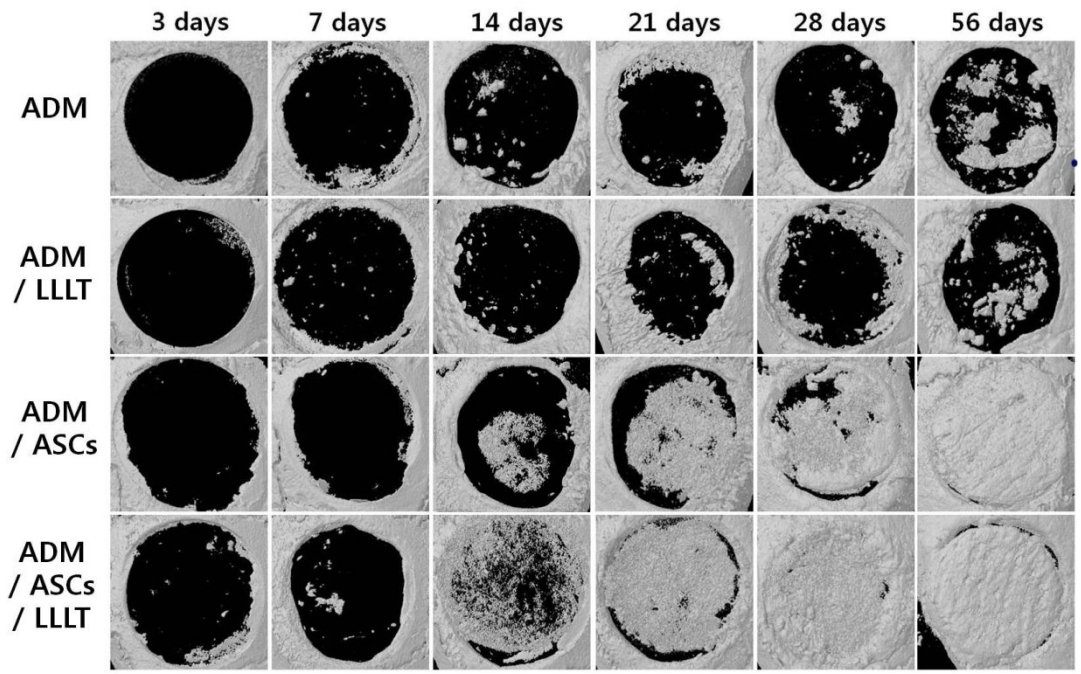

Fig. 2. Micro-CT evaluation. Micro-CT images of the critical-sized calvarial defect region in the ADM (top row), ADM/LLLT (second row), ADM/ASCs (third row) and ADM/ASCs/LLLT (bottom row) groups. These images are not from the same mice, but they are the most optimal images which could represent their osseous healing conditions of each experimental group at each harvested day (The diameter in all panels is 4 mm).

The value of bone mineral density (BMD) refers to the amount of mineral matter computed as mass per volume. The BMD at 3 days was approximately the same among all groups, but the BMD in the ADM/ASCs/LLLT group defects was significantly greater than that in the ADM, ADM/LLLT and ADM/ASCs groups defects after 7 days. At 14, 28 and 56 days, the BMD in the defects that received ADM/ASCs had a significant increase compared to the defects that received ADM and ADM/LLLT ($p < 0.05$) (Fig. 3a).

The total volume of bone tissue in the target defects was quantified as bone tissue volume (BTV). No significant difference of the BTV was found between the ADM and the ADM/LLLT groups defects. However, the BTV in the ADM/ASCs/LLLT group defects was significantly higher compared to the ADM, ADM/LLLT and ADM/ASCs groups defects after 7 days. The defects in the ADM/ASCs group showed higher BTV than those in the ADM and ADM/LLLT groups after 14 days ($p < 0.05$) (Fig. 3b).

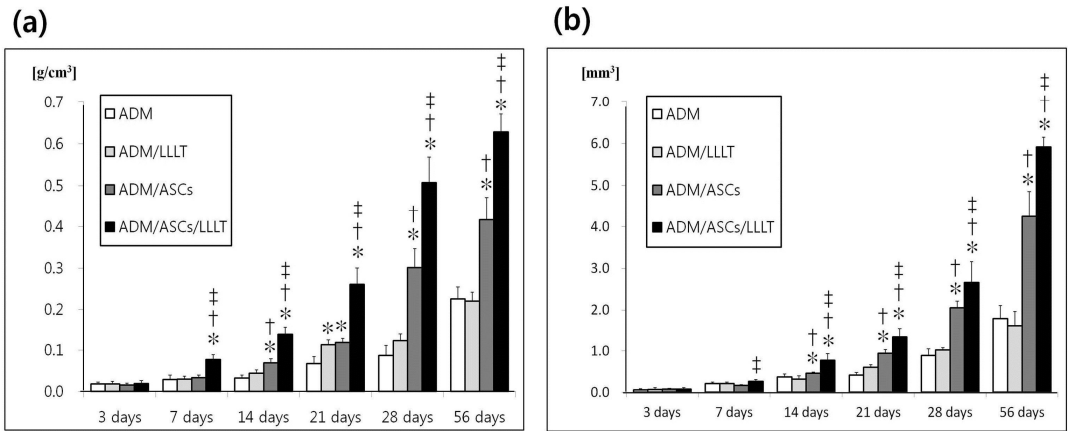

Fig. 3. Quantitative analysis of micro-CT images. BMD (a), BTV (b) from 3-56 days postoperatively. $^{*}p < 0.05$, indicating a significant difference compared to the ADM group; $^{\dagger}p < 0.05$, indicating a significant difference compared to the ADM/LLLT group; $^{\ddagger}p < 0.05$, indicating a significant difference compared to the ADM/ASCs group. Bars indicate means ± SD.

3. Proliferation and survival of ASCs in grafts

The proliferation and the survival of the ASCs in the grafts were confirmed by counting the ASCs, Ki67-, and TUNEL-positive ASCs using fluorescent microscopy throughout the ADM at 14 days. In the ADM/ASCs and the ADM/ASCs/LLLT groups, CM-DiI-labeled ASCs were identified as red fluorescence. As shown in Figures 4 and 5a (Fig. 4 and 5a), the ADM/ASCs/LLLT group (134.13 ± 4.53 ASCs/×200 field) exhibited significantly increased proportions of red fluorescent ASCs compared with the ADM/ASCs group (45.00 ± 3.89 ASCs/×200 field). The ratio of Ki67-positive cells of the ADM/ASCs/LLLT group (14.22 ± 2.67%) was found to be significantly greater than that of the ADM/ASCs group (9.64 ± 1.68%) (Fig. 5b). The ADM/ASCs/LLLT group had a lower percentage of TUNEL-positive cells (3.08 ± 0.52%) compared to the percentage of TUNEL-positive cells in the ADM/ASCs group (10.94 ± 3.30%) (Fig. 5c).

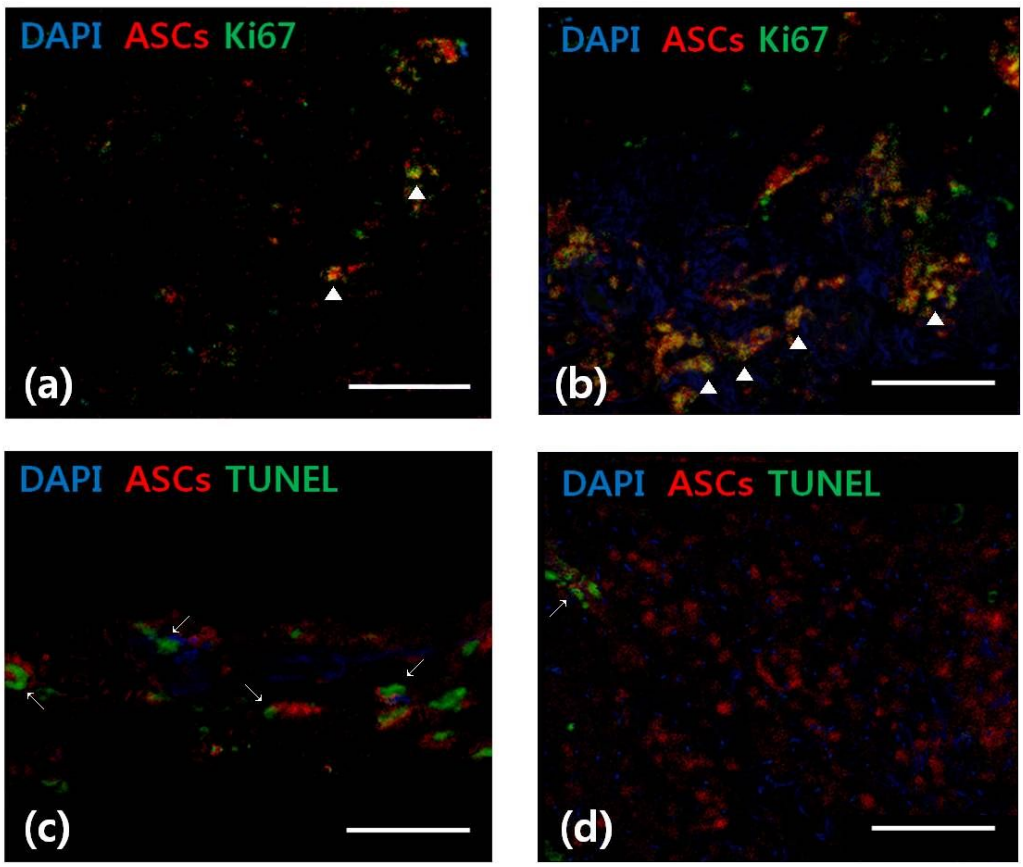

Fig. 4. Representative confocal images at 14 days. Ki67-positive cells are indicated by arrowheads in the ADM/ASCs (a) and ADM/ASCs/LLLT (b) groups. TUNEL-positive cells are indicated by arrows in the ADM/ASCs (c) and ADM/ASCs/LLLT (d) groups (Scale bar = 50 μm).

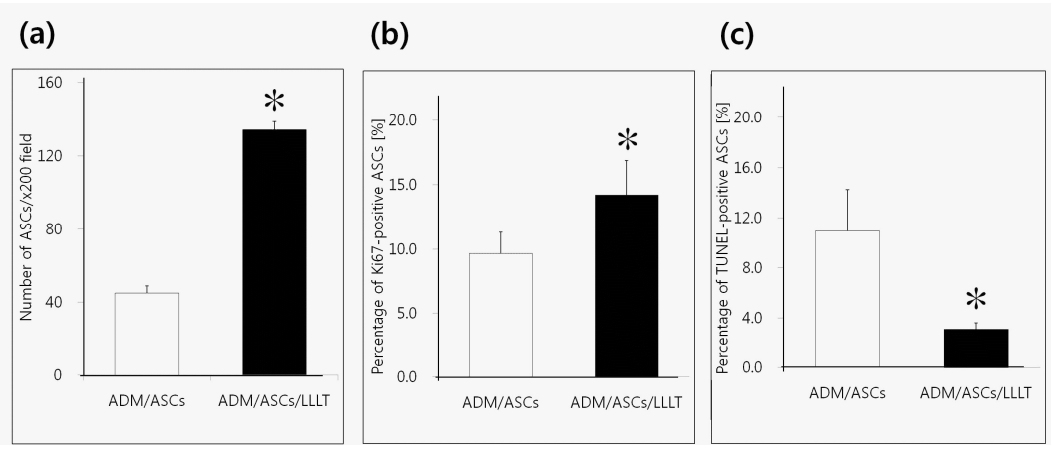

Fig. 5. Quantification of ASCs at 14 days. Number of ASCs per x200 field (a) was confirmed. Ki67-positive ASCs (b) and TUNEL-positive ASCs (c) were determined as a percentage at x200 field. $^{*}p < 0.05$, indicating a significant difference compared to the ADM/ASCs group. Bars indicate means ± SD.

4. Histological analysis

The histological observation of H&E staining showed that bone regeneration was more obvious in the ADM/ASCs and the ADM/ASCs/LLLT groups compared with the ADM and the ADM/LLLT groups (Fig. 6 and 7). The ADM and the ADM/LLLT groups showed a small amount of new bone deposition, scattered islands of woven bone and some loose connective tissue within the defects at 28 and 56 days. Many parts of the ADM were left in their original condition and did not convert to bony regenerate. In contrast, there was an increased amount of new bone formed within the defects of the ADM/ASCs group at 28 days, causing a thickened appearance with a well-formed trabeculae in the defect. A mixture of woven and lamellar bone was present, and more osteocytes were observed in the ADM/ASCs group. Blood vessels were occasionally observed, but very few parts of the grafts still maintained their original shape at 56 days. The ADM/ASCs/LLLT group displayed new bone deposition with evidence of a thick and complete bone trabeculae at 28 and 56 days. Many blood vessels and osteocytes were observed on the newly formed bone matrix. The bony edges appeared viable with osteoblasts and osteoclasts in their lacunae. Few parts of the scaffolds maintained at 28 days, but the original condition of the ADM was no longer present at 56 days.

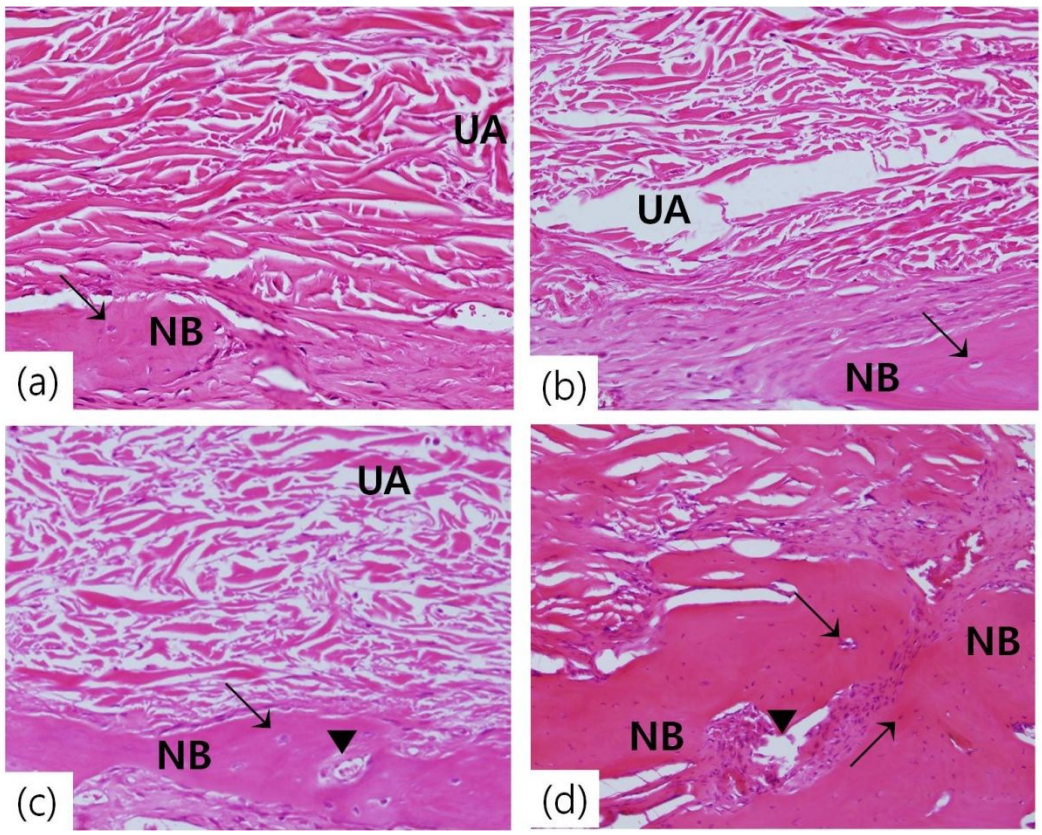

Fig. 6. Representative histology data of H&E stained samples obtained 28 days after surgery. Defects in the ADM (a), ADM/LLLT (b), ADM/ASCs (c) and ADM/ASCs/LLLT (d) groups (NB: new bone, UA: undegraded ADM, arrows: osteocytes, arrowheads: blood vessels, scale bar = 100 μm).

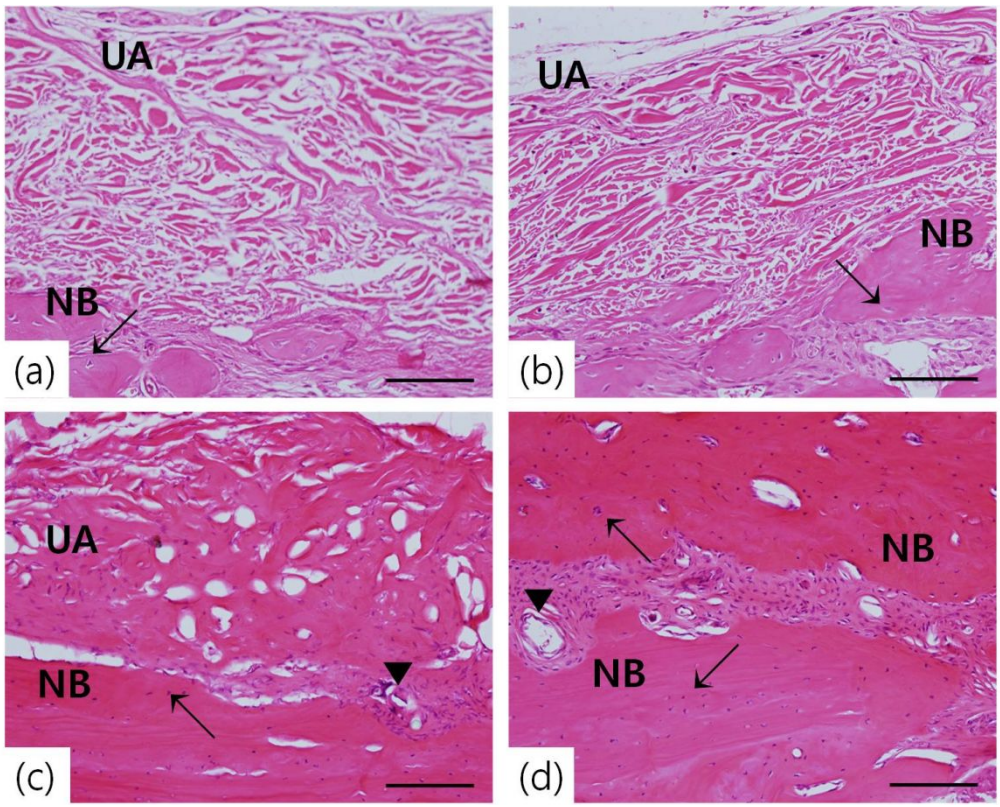

Fig. 7. Representative histology data of H&E stained samples obtained 56 days after surgery. Defects in the ADM (a), ADM/LLLT (b), ADM/ASCs (c) and ADM/ASCs/LLLT (d) groups (NB: new bone, UA: undegraded ADM, arrows: osteocytes, arrowheads: blood vessels, scale bar = 100 μm).

The results of immunohistochemistry and TRACP staining are shown in Figure 8 (Fig. 8). A positive purplish-red color for TRACP and the immunoreactions for bALP, OPN and OCA were found around the edges of bony regenerate, as well as on the newly made bone matrix in each group at 56 days. The stained cells along the bone tissue in the ADM/ASCs/LLLT group were strongly positive for bALP, OPN and OCA. The proportion of cells stained positive in the ADM/ASCs/LLLT group was higher than that in the other groups at 56 days. In comparison, the immunoreactions for bALP, OPN and OCA in the ADM/ASCs group were weaker than that in the ADM/ASCs/LLLT group, but stronger than that in the ADM and the ADM/LLLT groups at 56 days. In the ADM/ASCs/LLLT group, many parts of the defects were stained purplish-red color for TRACP, and the proportion of positive purplish-red color cells was higher than that in the other groups at 56 days. Additionally, the proportion of the positive-stained cells for TRACP in the ADM/ASCs group was greater compared with the ADM and the ADM/LLLT groups.

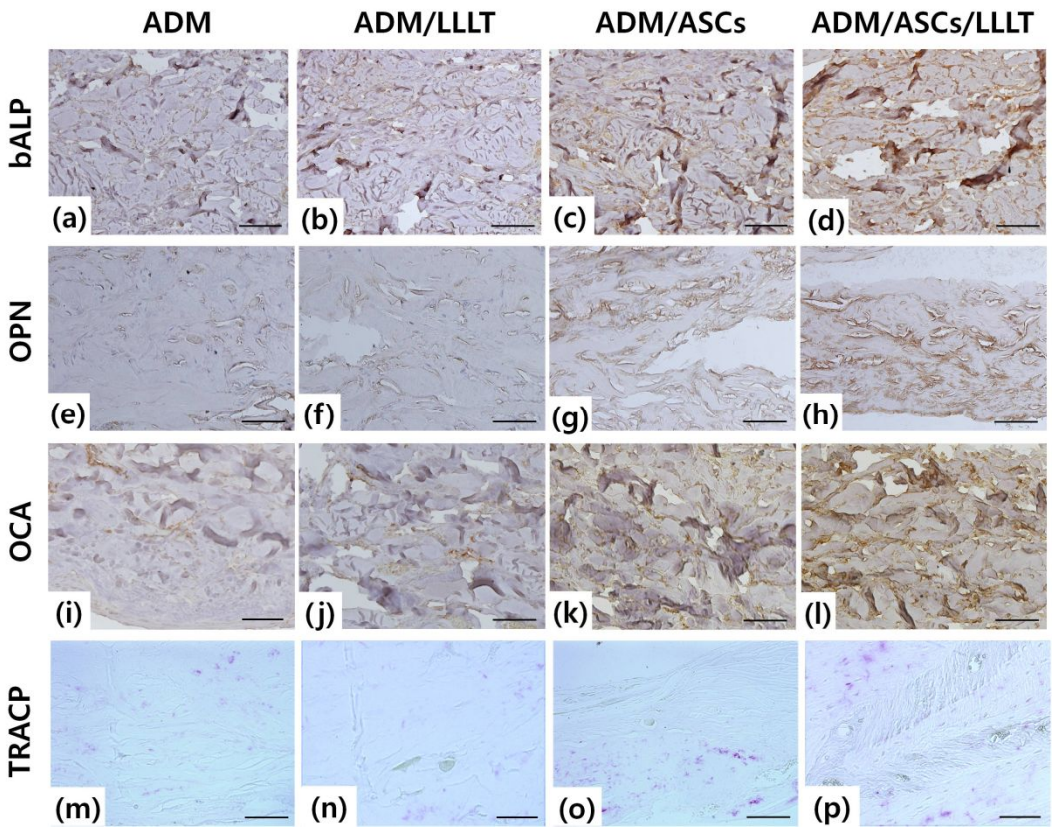

Fig. 8. Immunohistochemical analysis and TRACP staining of mouse calvarial defects 56 days after surgery. The panels show representative images of bALP (a-d), OPN (e-h), OCA (i-l), and TRACP (m-p) obtained from center of calvarial defect (Scale bar = 100 μm).

5. Analysis of osteogenic protein markers

The relative intensity of bALP secreted in the ADM/ASCs/LLLT group increased continuously, but decreased from 28 to 56 days (Fig. 9b). Additionally, the relative intensity of bALP in the ADM/ASCs/LLLT was significantly higher compared with the ADM, ADM/LLLT and ADM/ASCs groups after 3 days. The defects in the ADM/ASCs group showed higher relative intensity than those in the ADM and ADM/LLLT groups after 7 days.

The relative intensity of OPN and OCA in the ADM/ASCs/LLLT group was significantly greater compared with the ADM, ADM/LLLT and ADM/ASCs groups after 14 days. The ADM/ASCs group defects had a significant increase in the relative intensity of OPN and OCA compared to the ADM and the ADM/LLLT groups defects after 28 days (Fig. 9c and 9d).

As shown in figure 9e (Fig. 9e), the relative intensity of TRACP in the ADM/ASCs/LLLT group was significantly higher compared with the ADM, ADM/LLLT and ADM/ASCs groups at 14, 28 and 56 days. The ADM/ASCs group defects exhibited significantly greater relative intensity than the ADM and the ADM/LLLT groups after 28 days.

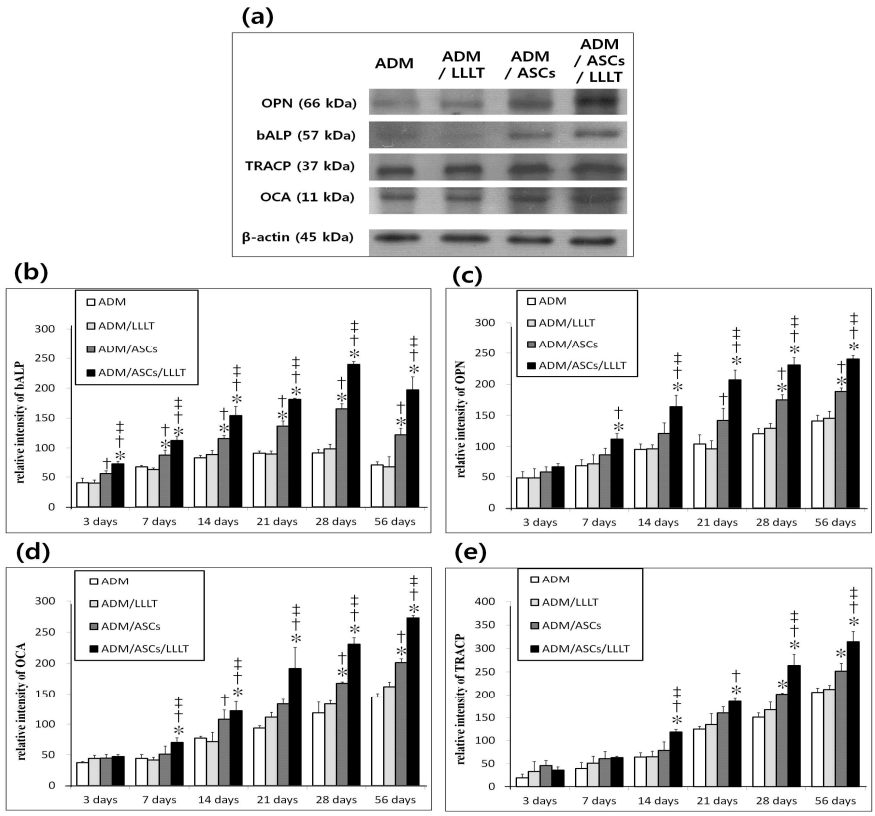

Fig. 9. Evaluation of osteogenic protein markers. Western blot assay shows expression of bALP, OPN, OCA and TRACP 56 days after surgery (a). The results of a western blot assay for bALP (b), OPN (c), OCA (d) and TRACP (e) were evaluated as relative intensity from 3-56 days postoperatively. $^{*}p < 0.05$, indicating a significant difference compared to the ADM group; $^{\dagger}p < 0.05$, indicating a significant difference compared to the ADM/LLLT group; $^{\ddagger}p < 0.05$, indicating a significant difference compared to the ADM/ASCs group. Bars indicate means ± SD.

IV. Discussion

Our previous study evaluated whether an ASC-seeded ADM could regenerate bone tissue to repair calvarial bone defects (Kim et al. 2012b). We went beyond the scope of our previous study to confirm the initial phase of bone regeneration before 28 days. Moreover, this study showed an effect of LLLT on the ASCs *in vivo*. First, our data revealed that the ASC attached well on the ADM, as we originally intended, and the ADM was confirmed as an ideal scaffold that provides a matrix to allow ingrowth of the seeded ASCs for bone regeneration in the animal model.

Our findings demonstrate that very little osseous tissue formation could be observed from the cutting edge of the surrounding normal bone at 3 days. However, the ADM/ASCs/LLLT group at 7 days and the ADM/ASCs group at 14 days showed that small bone islands and peninsulas were formed even in the center of the defects, and remarkable bone healing was observed in 3D imaging. This result may suggest that the osteogenic potential of ASCs, the ability to promote osteoprogenitor proliferation and the secretion of bone morphogenic proteins and growth factors, was accelerated within the initial 14 days.

Some groups reported that a scaffold alone or a scaffold modified with additional factors is sufficient for bone regeneration (Clokie et al. 2002, Kim et al. 2012b). In contrast, other groups reported that no functional repair could be achieved without seeding cells by a tissue engineering approach (Cui et al. 2007, Levi et al. 2010, Meinel et al. 2005). In our study, very small bony-union and scattered bone islands were found in the ADM and the ADM/LLLT groups. This result indicated that native mouse cells with an osteogenic potential could migrate to the ADM and form new bone in very small calvarial defects. However, the amount of native cells and the proportion of migrating cells might not be sufficient to arouse new bone for closing the critical-sized defects. After degradation of the ADM which was likely degraded over 56 days under original condition, not bony tissue but scar tissue would cover the defect in the ADM and the ADM/LLLT groups. In contrast, the ADM seeded with ASCs could secret growth factors to facilitate native cell migration to the defect and provide osteogenic cell sources for forming new bone. These facts may supported by greater relative intensity of bALP, OPN, OCA and TRACP as well as higher BMD and BTV scores in the ADM/ASCs and the ADM/ASCs/LLLT groups. As above, the ASCs in calvarial defects were evaluated to provide osteogenic cell sources and enable osteogenic proteins to be expressed to aid bone regeneration. Furthermore, it was probable that new bone formation was induced by ASCs in early period: ASCs form the majority of the new

bony tissue in initial stage by being differentiated to osteogenic cells itself, as well as by secreting the growth factors to native cell.

Several studies in recent years observed a significant decrease in the number of ASCs at the bone defect or skin wound bed within the first 14 days. The mechanisms of the decline of implanted ASCs are not yet fully understood. It is likely that with the progression of the healing process, cytokines and cellular molecules favorable to ASCs survival by the inhibition of apoptosis (Levi et al. 2010, Wu et al. 2007). In this study, compared with the ADM/ASCs group, the ADM/ASCs/LLLT group showed an increasing number of ASCs, an increasing percentage of Ki67-positive ASCs and a decreasing percentage of TUNEL-positive ASCs at 14 days. Additionally, the ADM/ASCs/LLLT group defects observed more remarkable bone healing and had a significant increase in BMD and BTV compared to the ADM/ASCs group defects. Consistent with our data, LLLT may enhance the functionality as well as the survival and the proliferation of the ASCs implanted onto the ADM. This enhanced functionality in bone healing effect was judged as the effect of LLLT on transplanted ASCs related to produce the bony tissue rather than on native cells. Some studies have demonstrated the effectiveness of LLLT for enhancing the viability and the proliferation of stem cells (Abramovitch-Gottlib et al. 2005, AlGhamdi et al. 2012, Hou et al.

2008, Mvula et al. 2008, Stein et al. 2005). It is possible that LLLT may affect ASCs proliferation through promoting the membrane potential of mitochondria (Hawkins et al. 2006, Hu et al. 2007).

To determine the effect of LLLT to form osseous tissue in conditions without ASCs, the ADM and the ADM/LLLT groups were compared. Previous studies reported that He-Ne laser irradiation produced an elevated structural stiffness and an enhanced bone repair in rat tibia injuries (Yaakobi et al. 1996). Another study demonstrated the failure of laser irradiation on fracture healing *in vivo* (David et al. 1996). In our data, both the ADM and the ADM/LLLT groups indicated little osseous healing in the marginal region and a minor amount of bone islands in a small percentage, even at 56 days. Neither a thicker layer of bone nor a bridge between bone islands was found in the defects. This result suggests that LLLT itself did not play a role in healing the defect *in vivo* at low power density and short irradiation times. It may suggest that the power density of our experiment was sufficient to affect the ASC-seeded ADM; however, the power density was too low to induce a bone repair directly *in vivo* (David et al. 1996). The experimental conditions of LLLT in inducing the bone repair confirmed that power density and exposure times depend on the variable conditions, location and size of the bone defect. Laser exposure over a certain power and

time could affect bone regeneration (Al-Watban et al. 2007, AlGhamdi et al. 2012). One study proposed that the cumulative effect of a lower dose determined the stimulatory effect, whereas multiple exposures at a higher dose resulted in an inhibitory effect with more damage to cells *in vitro* (Hawkins et al. 2006). It is probable that continuous exposures at a higher dose cause additional stress, thus reducing the cell viability, ATP activity and cell proliferation; therefore, a specific combination of energy density and exposure time is necessary for the stimulatory effects of LLLT.

In conclusion, ASCs are essential to close the critical-sized bone defects, and a potential combinatorial use of ADM and ASCs accelerates bone healing; thus, ASCs represent a promising cell type for future translational efforts in the repair of skeletal defects. Additionally, an appropriate amount of LLLT enhanced bone regeneration by influencing the functionality as well as the survival and the proliferation of ASCs on the ADM. These results could finally lead to rapid and effective bone tissue formation. We believe that the ASC-seeded ADM-athymic nude mouse model is useful for the optimization of ASC-mediated calvarial bone regeneration; furthermore, the ability of LLLT to affect ASCs *in vivo* may suggest clinical approaches for skeletal tissue regeneration.

V. References

Abramovitch-Gottlib, L., Gross, T., Naveh, D., Geresh, S., Rosenwaks, S., Bar, I. and Vago, R. (2005), "Low level laser irradiation stimulates osteogenic phenotype of mesenchymal stem cells seeded on a three-dimensional biomatrix." *Lasers Med Sci*, 20(3-4), 138-146.

Al-Watban, F.A.H., Zhang, X.Y. and Andres, B.L. (2007), "Low-level laser therapy enhances wound healing in diabetic rats: a comparison of different lasers." *Photomed Laser Surg*, 25(2), 72-77.

AlGhamdi, K.M., Kumar, A. and Moussa, N.A. (2012), "Low-level laser therapy: a useful technique for enhancing the proliferation of various cultured cells." *Lasers Med Sci*, 27(1), 237-249.

Amaral, A., Parizotto, N. and Salvini, T. (2001), "Dose-dependency of low-energy HeNe laser effect in regeneration of skeletal muscle in mice." *Lasers Med Sci*, 16(1), 44-51.

Clokie, C.M.L., Moghadam, H., Jackson, M.T. and Sandor, G.K.B. (2002), "Closure of

critical sized defects with allogenic and alloplastic bone substitutes." *J Craniofac Surg*, 13(1), 111-121.

Cui, L., Liu, B., Liu, G., Zhang, W., Cen, L., Sun, J., Yin, S., Liu, W. and Cao, Y. (2007), "Repair of cranial bone defects with adipose derived stem cells and coral scaffold in a canine model." *Biomaterials*, 28(36), 5477-5486.

David, R., Nissan, M., Cohen, I. and Soudry, M. (1996), "Effect of low-power He-Ne laser on fracture healing in rats." *Lasers Surg Med*, 19(4), 458-464.

Gupta, D.M., Kwan, M.D., Slater, B.J., Wan, D.C. and Longaker, M.T. (2008), "Applications of an athymic nude mouse model of nonhealing critical-sized calvarial defects." *J Craniofac Surg*, 19(1), 192-197.

Hawkins, D. and Abrahamse, H. (2006), "Effect of multiple exposures of low-level laser therapy on the cellular responses of wounded human skin fibroblasts." *Photomed Laser Surg*, 24(6), 705-714.

Hawkins, D.H. and Abrahamse, H. (2006), "The role of laser fluence in cell viability, proliferation, and membrane integrity of wounded human skin fibroblasts following helium-neon laser irradiation." *Lasers Surg Med*, 38(1), 74-83.

Hou, J., Zhang, H., Yuan, X., Li, J., Wei, Y. and Hu, S. (2008), "In vitro effects of low-level laser irradiation for bone marrow mesenchymal stem cells: Proliferation, growth factors secretion and myogenic differentiation." *Lasers Surg Med*, 40(10), 726-733.

Hu, W.P., Wang, J.J., Yu, C.L., Lan, C.C.E., Chen, G.S. and Yu, H.S. (2007), "Helium–neon laser irradiation stimulates cell proliferation through photostimulatory effects in mitochondria." *J Invest Dermatol*, 127(8), 2048-2057.

Kang, B., Ryu, H., Park, S., Kim, Y., Woo, H., Kim, W. and Kweon, O. (2012), "Effect of Matrigel on the Osteogenic Potential of Canine Adipose Tissue-Derived Mesenchymal Stem Cells." *J Vet Med Sci*, 74(7), 827-836.

Khan, S.N., Cammisa Jr, F.P., Sandhu, H.S., Diwan, A.D., Girardi, F.P. and Lane, J.M. (2005), "The biology of bone grafting." *J Am Acad Orthop Surg*, 13(1), 77-86.

Kim, H., Choi, K., Kweon, O.K. and Kim, W.H. (2012a), "Enhanced wound healing effect of canine adipose-derived mesenchymal stem cells with low-level laser therapy in athymic mice." *J Dermatol Sci,* 68(3), 149-156.

Kim, H.J., Park, S.S., Oh, S.Y., Kim, H., Kweon, O.K., Woo, H.M. and Kim, W.H. (2012b), "Effect of acellular dermal matrix as a delivery carrier of adipose-derived mesenchymal stem cells on bone regeneration." *J Biomed Mater Res B Appl Biomater*, 100(6), 1645-1653.

Levi, B., James, A.W., Nelson, E.R., Vistnes, D., Wu, B., Lee, M., Gupta, A. and Longaker, M.T. (2010), "Human adipose derived stromal cells heal critical size mouse calvarial defects." *PLoS One*, 5(6), e11177.

Meinel, L., Fajardo, R., Hofmann, S., Langer, R., Chen, J., Snyder, B., Vunjak-Novakovic, G. and Kaplan, D. (2005), "Silk implants for the healing of critical size bone defects." *Bone*, 37(5), 688-698.

Mvula, B., Mathope, T., Moore, T. and Abrahamse, H. (2008), "The effect of low level laser irradiation on adult human adipose derived stem cells." *Lasers Med Sci*, 23(3), 277-282.

Park, S.S., Lee, Y.J., Lee, S.H., Lee, D., Choi, K., Kim, W.H., Kweon, O.K. and Han, H.J. (2012), "Functional recovery after spinal cord injury in dogs treated with a combination of Matrigel and neural-induced adipose-derived mesenchymal Stem cells." *Cytotherapy*, 14(5), 584-597.

Ryu, H.H., Lim, J.H., Byeon, Y.E., Park, J.R., Seo, M.S., Lee, Y.W., Kim, W.H., Kang, K.S. and Kweon, O.K. (2009), "Functional recovery and neural differentiation after transplantation of allogenic adipose-derived stem cells in a canine model of acute spinal cord injury." *J Vet Sci*, 10(4), 273-284.

Schönmeyr, B., Clavin, N., Avraham, T., Longo, V. and Mehrara, B.J. (2009), "Synthesis of a tissue-engineered periosteum with acellular dermal matrix and cultured mesenchymal stem cells." *Tissue Eng Part A*, 15(7), 1833-1841.

Stein, A., Benayahu, D., Maltz, L. and Oron, U. (2005), "Low-level laser irradiation promotes proliferation and differentiation of human osteoblasts in vitro." *Photomed Laser Surg*, 23(2), 161-166.

Wu, Y., Chen, L., Scott, P.G. and Tredget, E.E. (2007), "Mesenchymal stem cells enhance wound healing through differentiation and angiogenesis." *Stem Cells*, 25(10), 2648-2659.

Yaakobi, T., Maltz, L. and Oron, U. (1996), "Promotion of bone repair in the cortical bone of the tibia in rats by low energy laser (He-Ne) irradiation." *Calcif Tissue Int*, 59(4), 297-300.

Ye, J.H., Xu, Y.J., Gao, J., Yan, S.G., Zhao, J., Tu, Q., Zhang, J., Duan, X.J., Sommer, C.A. and Mostoslavsky, G. (2011), "Critical-size calvarial bone defects healing in a mouse model with silk scaffolds and SATB2-modified iPSCs." *Biomaterials*, 32(22), 5065-5076.

Zuk, P.A., Zhu, M., Ashjian, P., De Ugarte, D.A., Huang, J.I., Mizuno, H., Alfonso, Z.C., Fraser, J.K., Benhaim, P. and Hedrick, M.H. (2002), "Human adipose tissue is a source of multipotent stem cells." *Mol Biol Cell*, 13(12), 4279-4295.

VI. 국문초록

저용량 레이저 치료가 무세포성 진피 기질에 배양된 개 지방유래 중간엽줄기세포의 골재생에 미치는 영향

서울대학교 대학원

수의학과 수의외과학 전공

최 규 석

지방유래 중간엽줄기세포 (adipose-derived mesenchymal stem cells, ASCs)를 무세포성 진피 기질 (acellular dermal matrix, ADM)과 공배양하여 제작한 이식물 (scaffold)은 골재생에 유용하게 이용되고 있다. 또한, 저용량 레이저 치료 (low-level laser therpy, LLLT)가 골수복에 영향을 준다는 연구가 다수 보고 되고 있다. 본 연구에서는 무흉선 마우스에 있어서 ASCs와 공배양한 ADM을 LLLT와 함께 적용하여 두개골 결손창의 골재생 가능성을 조사하였다.

무흉선 마우스의 두개골에 직경 4 mm 크기의 골결손을 양측으로 유발하고, ADM만 적용한 군 (ADM 군), ADM만 적용하고 LLLT를 적용한 군 (ADM/LLLT 군), ASCs와 공배양 한 ADM을 적용한 군 (ADM/ASCs 군), ASCs와 공배양 한 ADM을 적용하고 LLLT를 적용한 군 (ADM/ASCs/LLLT 군)으로 무작위로 나누어 처치를 적용하였다. 3일, 7일, 14일, 21일, 28일, 56일차에 시료를 수거하였고, 미세 컴퓨터 단층촬영 (micro-CT)을 통한 삼차원 영상, 골밀도 (bone mineral density, BMD), 골조직용적 (bone tissue volume, BTV)을 분석하였으며, hematoxylin & eosin (H & E) 염색, 면역조직화학 염색 및 western blot을 통해서 골재생 효과를 분석하였다.

삼차원 영상에서는 14일차에 ADM/ASCs와 ADM/ASCs/LLLT 군에서 다른 군에 비해 유의적인 골형성이 확인되었고, ADM/ASCs/LLLT 군은 28일차에, ADM/ASCs 군은 56일차에 골재생이 전체적으로 명확하게 확인되었다. BMD, BTV에 대한 분석결과에서 ADM/ASCs/LLLT 군은 7일차 이후에, ADM/ASCs 군은 14일차 이후에 유의적인 증가가 확인되었다. 14일차에 Ki67, TUNEL에 대한 면역형광염색을 통해, 이식한 ASCs의 증식 및 생존성을 평가한 결과에서는 ADM/ASCs/LLLT 군에서 ADM/ASCs 군에 비해 증식 촉진 및 세포자멸사 억제 효과로 인한 생존성 증가가 확인되었고, 이를 통해 LLLT의 ASCs 증식 및 생존성 향상 효과를 확인하였다. 조직학적 분석에서는 ADM/ASCs 군과

ADM/ASCs/LLLT 군에서 골결손부의 수복이 확인되었지만, ADM 군과 ADM/LLLT 군의 경우에는 28일차, 56일차에도 소수의 연결성이 없는 골(bone island) 형성과 섬유소 연결만 확인되었다. 면역조직화학적 평가에서는 ASCs/ADM/LLLT 군에서 다른 군들에 비해 골형성 단백질의 유의적인 증가가 확인되었다.

ASCs와 공배양한 ADM은 골재생을 촉진시키고, LLLT의 추가 적용은 빠른 속도의 골재생으로 이어진다는 결과를 확인하였으며, 이를 토대로 손상된 골조직의 재생에 있어서 ASCs와 공배양한 ADM을 LLLT와 함께 적용하는 것이 효과적일 것이라 생각된다.

주요어: 저용량 레이저 치료, 지방유래 중간엽줄기세포, 무세포성 진피 기질, 골재생, 무흉선 마우스, 이식물
학 번: 2010 – 21634